Journal of Materials Chemistry A

RSC Publishing

PAPER

View Article Online
View Journal | View Issue

Improved thermoelectric properties in Zn-doped $Ca_5Ga_2Sb_6$

Cite this: *J. Mater. Chem. A*, 2013, **1**, 4244

Samantha I. Johnson, Alex Zevalkink and G. Jeffrey Snyder*

Zintl compounds with the chemical formula $Ca_5M_2Sb_6$ have attracted attention as candidates for use in thermoelectric applications due to their low thermal conductivity and promising high temperature performance (*i.e.*, $zT = 0.6$ at 1000 K in $Ca_5Al_{2-x}Na_xSb_6$). We have shown previously that, relative to $Ca_5Al_2Sb_6$, both $Ca_5Ga_2Sb_6$ and $Ca_5In_2Sb_6$ have reduced phonon velocities and improved carrier mobility, suggesting that improved zT can be achieved in these materials. Here we further investigate $Ca_5Ga_2Sb_6$, which is an intrinsic semiconductor with a small concentration of p-type carriers. By substituting Zn^{2+} on the Ga^{3+} site, we show that it is possible to increase and control the carrier concentration in $Ca_5Ga_{2-x}Zn_xSb_6$ and thus optimize its thermoelectric behavior. A single parabolic band model was used to estimate an effective mass of $m^* = 1.6m_e$, which is slightly lower than Al-based compounds. Though the reduced m^* leads to a lower Seebeck coefficient, it also leads to a much higher electronic mobility. The high mobility leads to increased thermoelectric figure of merit (zT) at low and intermediate temperatures relative to Zn-doped $Ca_5Al_2Sb_6$. However, due to the decreased band gap in $Ca_5Ga_2Sb_6$ relative to $Ca_5Al_2Sb_6$, the maximum zT in optimally doped $Ca_5Ga_2Sb_6$ is reduced (peak $zT \sim 0.35$ at $T = 775$ K).

Received 26th October 2012
Accepted 4th February 2013

DOI: 10.1039/c3ta00844d

www.rsc.org/MaterialsA

Introduction

Thermoelectric devices are able to directly convert heat to electricity, making them relevant to today's energy concerns. These devices are currently used for energy generation in deep-space missions and waste heat recovery in industry, and they have the potential to increase the overall efficiency of automobiles.[1] However, widespread use of thermoelectric materials has been limited by their poor efficiency.[2] The maximum efficiency of these materials is governed by the thermoelectric figure of merit, $zT = \frac{\alpha^2 T}{\rho\kappa}$, where α is the Seebeck coefficient, ρ is electrical resistivity, and κ is the thermal conductivity. To optimize zT, a careful balance between these properties must be found.[3]

The ideally engineered thermoelectric material has the electronic properties of a crystal and the low thermal conductivity of a glass, giving rise to the term "electron-crystal, phonon-glass".[4]

Zintl phases, characterized by covalently bonded anionic structures surrounded by ionically bonded cations, have been recently recognized as promising thermoelectric materials.[5] The need to satisfy valence often leads to incredibly complex structures, making many Zintl compounds natural "phonon glasses".[6,7] At the same time, the complex, often highly anisotropic, covalent structures can potentially be harnessed for electronic conduction, leading to the desired "electron crystal" behavior.[8,9]

Among Zintl compounds, a diverse array of polyanions can be found, ranging from isolated (0-dimensional) $MnSb_4$ tetrahedra and linear Sb trimers found in $Yb_{14}MnSb_{11}$, to the 3-dimensional, cage-like networks that characterize clathrate and skutterudite compounds. Excellent thermoelectric properties (zT greater than 1) have been demonstrated in compounds at both ends of this spectrum[11–14] as well as in compounds with 2-dimensional anionic structures (*i.e.*, AM_2Sb_2 compounds, where A = alkaline or rare earth metal and M = transition metal[15–18]).

Zintl compounds based on 1-dimensional anionic chains have only recently become of interest for thermoelectric applications. Ca_3AlSb_3, Sr_3GaSb_3, and $Ca_5Al_2Sb_6$ are a few examples, each forming a different crystal structure based on chains of corner-linked MSb_4 tetrahedra.[19–21] All are intrinsic semiconductors with low lattice thermal conductivity (<0.6 W m^{-1} K^{-1}) and promising high temperature thermoelectric properties ($zT > 0.6$) when optimally doped. Of these chain-forming crystal structures, that of $Ca_5Al_2Sb_6$ ($Ca_5Ga_2As_6$ structure type) is the most tolerant of chemical substitutions; Ga or In can substitute for Al, and Sr, Ba, or Eu, can substitute for Ca (in the In analogue).[19] The $Ca_5Ga_2As_6$ structure type, shown in Fig. 1 for $Ca_5Ga_2Sb_6$, is comprised of chains of corner-linked $GaSb_4$ tetrahedra. Neighboring chains are joined by Sb–Sb bonds to form infinite ladder-like structures. Valence counting in these anionic chains finds two Sb^{1-} bridging across the chains, two corner sharing Sb^{1-} linking tetrahedra along the

Materials Science, California Institute of Technology, 1200 E. California Boulevard, Pasadena, California 91125, USA. E-mail: jsnyder@caltech.edu

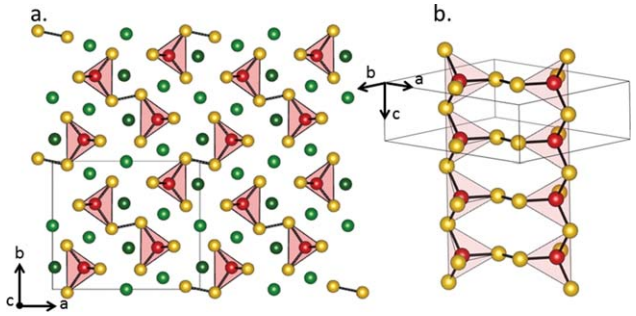

Fig. 1 (a) The crystal structure of $Ca_5Ga_2Sb_6$ (orthorhombic, *Pbam*) viewed down the tetrahedral chains. (b) The tetrahedral chains, viewed from the side, are linked by Sb–Sb bonds to form "ladders". Ca atoms are shown in green, Sb in yellow, and Ga in red.[10]

chain, and two Sb^{2-} that are covalently bonded only to the Ga. The two Ga atoms are each bonded to four antimony atoms, yielding a formal valence of −1. Surrounding the "ladders" are five Ca^{2+} cations, which provide overall charge balance.[22,23]

Our recent study comparing undoped $Ca_5M_2Sb_6$ compounds (M = Al, Ga, In) showed decreased phonon velocities and improved electronic mobility in the undoped Ga and In analogues relative to undoped $Ca_5Al_2Sb_6$.[24] This motivates us to study $Ca_5Ga_2Sb_6$, despite the disadvantage of the increased cost of Ga relative to Al. $Ca_5Ga_2Sb_6$, like the Al analogue, requires doping to optimize its electronic properties and realize its maximum possible zT. We have previously shown that $Ca_5Al_2Sb_6$ can be doped with Na on the Ca site, or with Zn or Mn on the Al site to increase the p-type carrier concentration, thereby drastically improving the zT.[25,26] Zn doping yielded the best control of the carrier concentration, and is therefore used here. This study explores the properties of $Ca_5Ga_{2-x}Zn_xSb_6$, with x ranging from 0 to 0.3. We use a combination of high temperature electronic and thermal transport measurements and simple modeling assuming a single parabolic band to characterize and optimize the thermoelectric properties of this system.

Experimental

$Ca_5Ga_{2-x}Zn_xSb_6$ samples with x = 0.05, 0.1, 0.2, 0.3 were prepared for this study. For undoped $Ca_5Ga_2Sb_6$ (x = 0), we present data from our prior work.[24] The initial GaSb precursor was formed from 99.99% Ga shot and 99.9999% Sb shot, which was mixed in equimolar amounts and vacuum sealed in a quartz tube. The mixture was held at 973 K for 12 hours and then quenched in water. The GaSb was subsequently crushed and mixed with stoichiometric amounts of 99.99% Ca dendrites, 99.99% Zn shot, and 99.9999% Sb shot from Sigma Aldrich and loaded into stainless steel vials with stainless steel balls in an argon-filled glove box. The mixture was milled for 1 h in a SPEX Sample Prep 8000 Series Mixer/Mill. The resulting powder was pressed in graphite dies (from POCO) in argon. Before pressing, the powder was held at the minimum load at 873 K for 2 h to ensure complete reaction of the GaSb. The powder was then consolidated at 973 K under 110 MPa of pressure for 3 h followed by a 2 h stress-free cool down.

For comparison, an Al-based sample ($Ca_5Al_{1.9}Zn_{0.1}Sb_6$) was also synthesized for this study. The Al-based reference sample was synthesized using the method described in,[25] with one exception: the hot pressing temperature was increased from 873 K to 1073 K. This change was made to correct for the extremely low mobility in our initial study of Zn-doped $Ca_5Al_2Sb_6$.[25]

The resulting polycrystalline samples were sliced into disks 1 mm thick and 12 mm in diameter. X-ray diffraction was performed on the disks using a Philips XPERT MPD diffractometer operating at 45 kV and 40 mA. Rietveld analysis was completed using Phillips XPERT Plus software. Scanning electron microscopy and electron dispersive spectroscopy were performed with a Zeiss 1550 VP SEM. High temperature resistivity data was taken up to 850 K using the van der Pauw technique. Hall data was measured in a 2 T magnetic field using pressed niobium contacts.[27] Seebeck data was taken using Chromel–Nb thermocouples and by oscillating the temperature gradient ±10 K.[28] Thermal diffusivity was collected using a Netzsch LFA 457. The temperature of measurements was limited to 873 K because of the thermal instability of the $Ca_5Ga_{2-x}Zn_xSb_6$ observed above this temperature. The combined measurement uncertainty in the thermoelectric figure of merit (zT), is generally given as 20%.

Results and discussion

The phase purity of the $Ca_5Ga_{2-x}Zn_xSb_6$ (x = 0, 0.05, 0.1, 0.2, 0.3) samples and the reference sample was determined by XRD and SEM. Representative patterns of the x = 0 and x = 0.3 samples can be seen in Fig. 2. A simulated Rietveld fit using the reported crystal structure is also shown underneath.[22] The reflection denoted by an asterisk in the undoped sample is a secondary phase, identified as $CaSb_2$ using EDS. In all of the $Ca_5Ga_{2-x}Zn_xSb_6$ (x = 0, 0.05, 0.1, 0.2, 0.3) samples, a small fraction (~1 volume%) of this secondary phase was observed

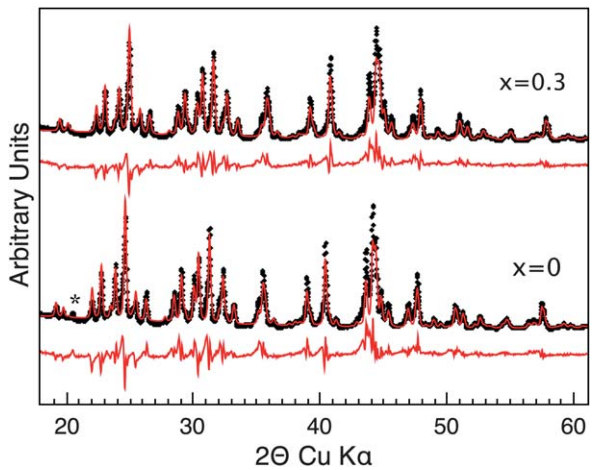

Fig. 2 XRD patterns of $Ca_5Ga_{2-x}Zn_xSb_6$ (x = 0 and x = 0.3) are shown in black. A small amount of the secondary phase $CaSb_2$ was observed in all samples. In the sample with x = 0, the asterisk denotes a reflection from $CaSb_2$. The simulated Rietveld fits are overlaid in red, and the difference profile is shown in red underneath.[23]

during SEM analysis (visually determined from the estimated ratio of the $CaSb_2$ area to that of the matrix phase). The $CaSb_2$ content does not appear to increase with Zn concentration. The geometric density of the samples ranges from 97–98% of the theoretical density, and grain sizes for the samples, estimated from SEM analysis of fracture surfaces, range from 1–5 μm.

Electronic transport properties

Our initial investigation of the $Ca_5M_2Sb_6$ compounds (M = Al, Ga, In) revealed non-degenerate semiconducting behavior and low p-type carrier concentration ($\sim 10^{18}$ h^+ per cm^3) in all three compounds.[24] Relative to the Al- and In-based compounds, $Ca_5Ga_2Sb_6$ samples exhibited both a reduced band gap (E_g), determined from high temperature resistivity and Seebeck measurements, and improved hole mobility. These experimental results were consistent with density functional theory (DFT) calculations, which predicted a lighter valence band effective mass (m^*) and a smaller E_g ($\sim$0.4 eV) arising from the low energy (relative to Al–Sb or In–Sb) Ga–Sb anti-bonding states at the conduction band edge.[24] In thermoelectric materials, light m^* and the corresponding high mobility are desirable,[29] while a small band gap can be detrimental, particularly at high temperature materials.

To optimize the electronic properties of $Ca_5Ga_2Sb_6$, electronic doping is necessary. Motivated by the successful use of Zn^{2+} as a dopant to replace Al^{3+} in $Ca_5Al_2Sb_6$,[25] here we substitute Zn^{2+} on the Ga^{3+} site. Simple valence counting predicts that each Zn substitution will yield one free hole. This simple assumption is accurate at low Zn concentrations, as illustrated by the inset in Fig. 3a. The room temperature Hall carrier concentration, n_H, is similar to the theoretical carrier concentration, n (dashed line) for $x < 0.2$, but diverges when $x > 0.3$. This divergence might be explained by a low solubility of Zn in this system or by the formation of compensating n-type defects. The highest achieved n_H is $\sim 6 \times 10^{20}$ h^+ per cm^3, which is significantly higher than the maximum n_H obtained in Zn-doped $Ca_5Al_2Sb_6$. The ability to dope $Ca_5Ga_2Sb_6$ to a greater extent than $Ca_5Al_2Sb_6$ may result from Ga compound's smaller band gap; this may permit a Fermi level further from the valence band edge before the system forms compensating defects.[30] Additionally, the more closely matched ionic radii of the Ga and Zn atoms may allow for a larger solubility of Zn, and thus higher maximum doping levels compared to the Al compound.

As the Hall carrier concentration increases in magnitude, the temperature dependence exhibits a transition from intrinsic to extrinsic semiconducting behavior, as shown in Fig. 3a. In the undoped sample, n_H increases exponentially due to intrinsic carrier activation, resulting in a change in the majority carrier type above 650 K (unfilled blue symbols indicate negative data). This explanation relies on the assumption that the electrons have higher mobility than the holes, and thus dominate the Hall coefficient. A detailed discussion of this behavior can be found in Zevalkink *et al.*[24] In contrast, the temperature independent carrier concentrations of the doped samples are indicative of metallic behavior with transport dominated by extrinsic carriers. For comparison, we have included a representative $Ca_5Al_{2-x}Zn_xSb_6$ sample with $x = 0.1$. In both the Al and Ga analogues with $x = 0.1$, the carrier concentration values and trends are in agreement.

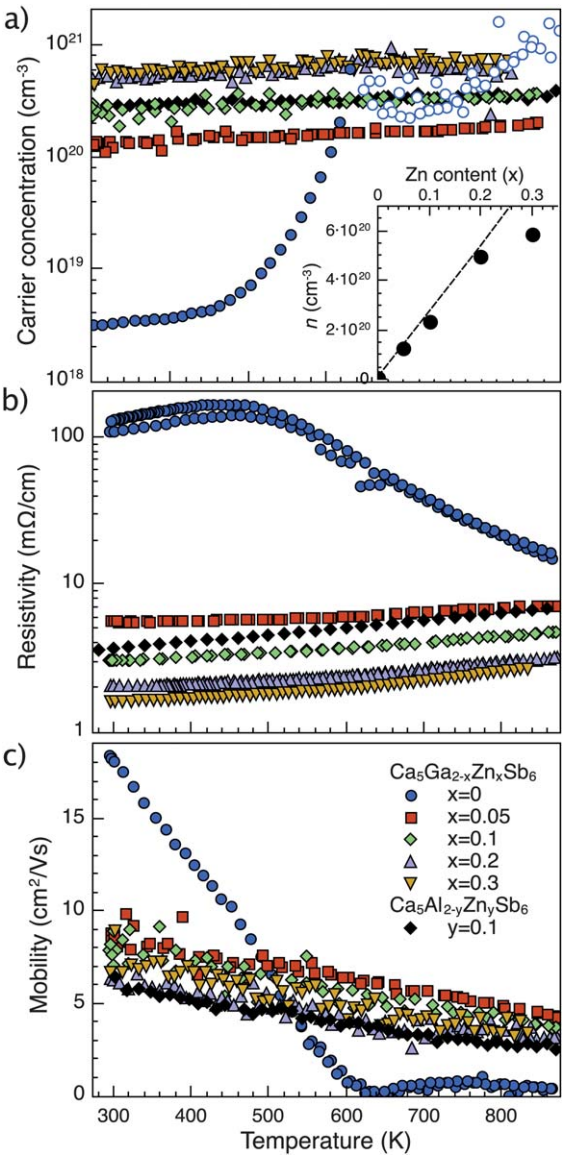

Fig. 3 (a) The Hall carrier concentration, n_H, increases with increased Zn content, x. Inset: n_H begins to deviate from the expected values shown by the dashed line. (b) Resistivity decreases with increasing n_H, showing a transition from intrinsic semiconducting to metallic behavior. (c) Hall mobility decreases with increasing x, but is improved relative the Al-analogue, $Ca_5Al_{1.9}Zn_{0.1}Sb_6$.

As shown in Fig. 3b, with increasing x, the resistivity (ρ) decreases by nearly two orders of magnitude due to the increase in hole concentration. In the doped samples, resistivity increases with temperature due to decreasing hole mobility (Fig. 3c). In contrast, the undoped sample has resistivity that *decreases* with temperature due to the competing effect of intrinsic carrier activation. As discussed in ref. 24, a reversible discontinuity in the data around 600 K (also observed in $Ca_5In_2Sb_6$) may be due to a phase transition. The resistivity of $Ca_5Al_{1.9}Zn_{0.1}Sb_6$ is shown for comparison.

The Hall mobility (μ), calculated from $\rho = 1/ne$, is shown in Fig. 3c. At room temperature, μ in the undoped sample is more than twice that of the doped samples. The mobility of the doped samples, in general, decreases with increasing x, though still remains higher than observed in either Na- or Zn-doped $Ca_5Al_2Sb_6$. Note that the Al-based reference sample synthesized for this study has higher mobility than the samples in our previous report on Zn-doped $Ca_5Al_2Sb_6$.[25] This may be due to improved microstructure (larger grain size) resulting from the increased hot pressing temperature used in the current study. Compared with $Ca_5Al_{1.9}Zn_{0.1}Sb_6$, the mobility of $Ca_5Ga_{1.9}Zn_{0.1}Sb_6$ is improved by ~20%, which is beneficial to the compound's performance and figure of merit. In all doped samples, the temperature dependence of μ_H is indicative of acoustic phonon scattering (described by $\mu \propto T^{-\upsilon}$, where υ ranges from 1 to 1.5 for degenerate and non-degenerate semiconductors, respectively).[31] For all Zn-doped samples in this study, υ ranges from 1.3 to 1.7. Note that the near-zero mobility above 600 K in the undoped sample stems from the assumption of a single carrier type, and does not represent the true drift mobility of the holes.

The Seebeck coefficients (α) are shown in Fig. 4 up to 873 K. The undoped sample displays a large room temperature Seebeck coefficient characteristic of a nondegenerate semiconductor. It then rapidly decreases with increasing temperature due to the thermally activated minority carriers observed in the Hall effect. With increasing x, the Seebeck coefficients decrease and exhibit increasingly linear temperature dependences. Relative to $Ca_5Al_{2-x}Zn_xSb_6$ (plotted for x = 0.10 case), the reduction of α in $Ca_5Ga_{2-x}Zn_xSb_6$ samples due to minority carriers begins at lower temperature. The magnitude and temperature at which the Seebeck coefficient peaks (α_{max} and T_{max}) can be used to roughly estimate the band gap using $E_g = 2e\alpha_{max}T_{max}$.[32] This estimate yields E_g = 0.2–0.3 eV, in contrast to the larger estimate of 0.4 eV in $Ca_5Al_2Sb_6$.[19]

The relationship between α and n_H (shown in Fig. 5) is well described by a single parabolic band model (SPB), assuming an effective mass of $1.6m_e$ and that acoustic phonons are the primary scattering source. A more detailed description of this model can be found in ref. 13 and 19. A single band model cannot account for minority carriers effects at high temperature, and is thus only used to 500 K. Consistent with prior DFT results, which predicted a lighter valence band in $Ca_5Ga_2Sb_6$ relative to both the In and Al analogues, our experimental effective mass of $1.6m_e$ is significantly lower than that observed in $Ca_5Al_2Sb_6$ samples ($2.2m_e$). In all $Ca_5M_2Sb_6$ compounds, the calculated band structures predict significant deviations from parabolic behavior when the Fermi energy is far from the band edge, as expected from heavy doping. Since $Ca_5Ga_2Sb_6$ can be doped to higher hole concentrations than the Al analogue, it provides an opportunity to experimentally probe deeper into the valence band. However, we are unable to confirm the expected non-parabolic behavior, as even the most heavily doped samples are reasonably well described by a constant effective mass, within experimental error.

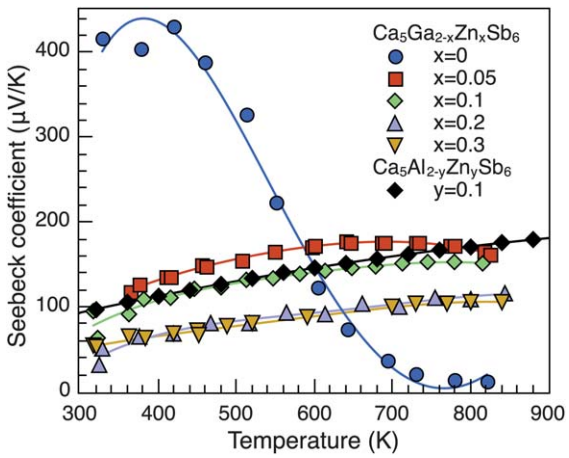

Fig. 4 With increasing Zn content, the Seebeck coefficient of $Ca_5Ga_{2-x}Zn_xSb_6$ decreases in magnitude and exhibits an increasingly linear temperature dependence. A $Ca_5Al_{2-y}Zn_ySb_6$ sample (y = 0.1) is included for comparison.

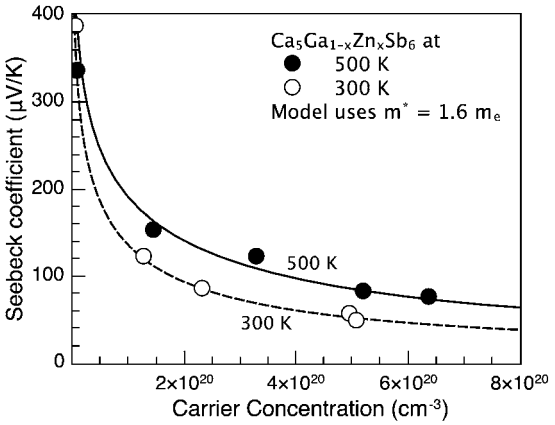

Fig. 5 The experimental Seebeck coefficients of $Ca_5Ga_{2-x}Zn_xSb_6$ *versus* carrier concentration at T = 300 and 500 K are compared with a single parabolic band (SPB) model, showing general agreement. An effective mass of $1.6m_e$ was used for both temperatures.

Thermal transport properties

The total thermal conductivity, shown in Fig. 6a, is calculated from the measured thermal diffusivity (D) according to the equation $\kappa_{total} = C_pDd$, where in this case d is the geometric density and C_P is the Dulong–Petit heat capacity. Note that our use of the Dulong–Petit heat capacity may underestimate the heat capacity, and thus the thermal conductivity, by 10–20% at very high temperatures. The total thermal conductivity is the sum of three components: the electronic (κ_e), bipolar (κ_B), and lattice (κ_L) contributions. The electronic component has been estimated from the Wiedemann–Franz equation, $\kappa_e = \frac{LT}{\rho}$, where L is the Lorenz number calculated using the SPB model (shown in the inset in Fig. 6). Thus, the total thermal conductivity tends to increase with increasing dopant concentration, as ρ decreases. Comparison with the x = 0.1 case of $Ca_5Al_{2-x}Zn_xSb_6$ is shown as well.

Lattice thermal conductivity (Fig. 6b) is obtained by subtracting κ_e from κ_{total}, providing that the bipolar contribution is

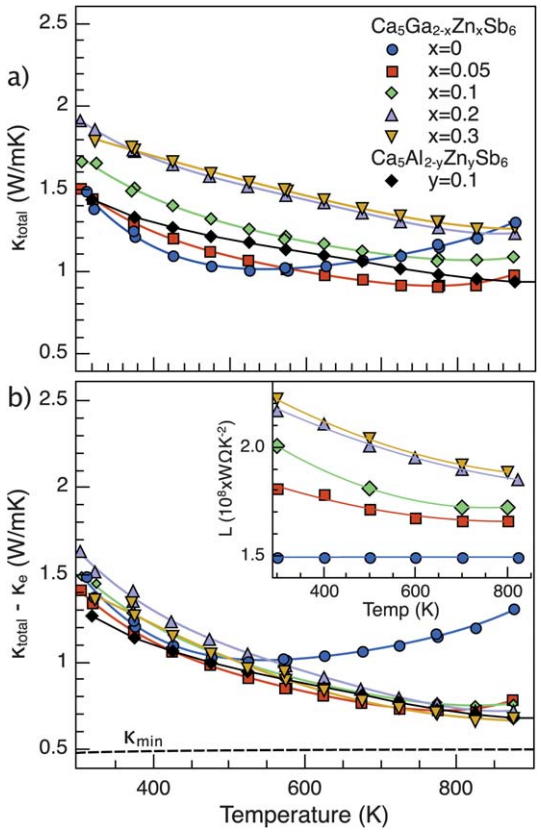

Fig. 6 (a) The total thermal conductivity in $Ca_5Ga_{2-x}Zn_xSb_6$ increases with increasing x. (b) Subtracting the electronic contribution yields the lattice and bipolar contributions to the thermal conductivity, the latter of which is most apparent in the undoped sample ($x = 0$). The inset displays the Lorenz number, calculated from the SPB model using experimental Seebeck coefficients.

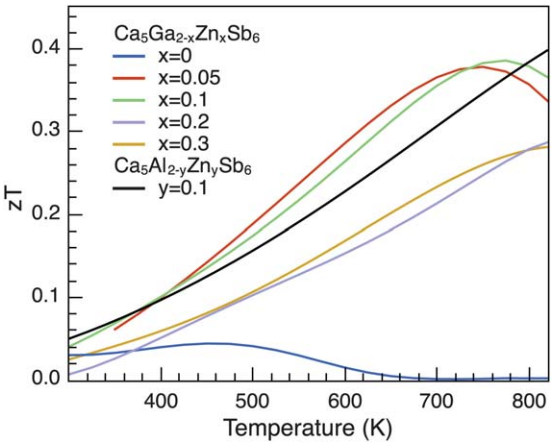

Fig. 7 The figure of merit of $Ca_5Ga_{2-x}Zn_xSb_6$ reaches a maximum of ~0.35 at 750 K for samples with $x = 0.05$ and $x = 0.1$. Relative to the Al analogue, the average zT is somewhat improved between 400 and 800 K (increased from 0.23 to 0.26). The magnitude and temperature of the peak zT are reduced relative to the Al analogue due to the smaller band gap in $Ca_5Ga_2Sb_6$.

negligible. This is clearly not the case for the undoped material, in which $\kappa_{total} - \kappa_e$ rises with temperature above 600 K, indicating that there is a significant bipolar contribution. In contrast, the Zn-doped samples show no obvious indication of a bipolar contribution; in these, $\kappa_{total} - \kappa_e$ decreases with temperature approximately as $1/T$, characteristic of lattice thermal conductivity limited by Umklapp phonon–phonon scattering.[7]

The minimum lattice thermal conductivity (κ_{min})[33,34] places a theoretical lower limit on κ_L, which derives from the minimum allowed scattering distance ($l = \lambda/2$) for phonons with wavelength λ. At high temperatures, κ_{min} can be approximated by eqn (1), where V is the average volume per atom and ν_T and ν_L are the transverse and longitudinal sound velocities, respectively. Ultrasonic measurements of ν_T and ν_L for undoped $Ca_5M_2Sb_6$ compounds (M = Al, Ga, In) are detailed in ref. 24. Relative to $Ca_5Al_2Sb_6$, the higher density and lower stiffness in $Ca_5Ga_2Sb_6$ lead to lower speed of sound, and thus lower

$$\kappa_{min} = \frac{1}{2}\left(\frac{\pi}{6}\right)^{1/3} k_B V^{-2/3}(2\nu_T + \nu_L). \quad (1)$$

The dashed line in Fig. 6b denotes the estimated κ_{min} for $Ca_5Ga_2Sb_6$. Unlike in doped $Ca_5Al_2Sb_6$ samples (of which the $x = 0.10$ case is plotted), which actually reach the predicted κ_{min} at high temperatures, κ_L in Zn-doped $Ca_5Ga_2Sb_6$ remains conspicuously high. This may suggest that a small, but not negligible, bipolar contribution is present even in the most heavily Zn-doped samples. This is likely an additional adverse effect of the small band gap in $Ca_5Ga_2Sb_6$, limiting the potential of this compound for high temperature applications.

Figure of merit

The figures of merit for $Ca_5Ga_{2-x}Zn_xSb_6$ samples, calculated using polynomial fits to the experimental data, are shown in Fig. 7. At low temperatures, the effect of the increased mobility in the Ga compound dominates, leading to an apparent improvement in zT from 400 to 750 K relative the Al-based material. This may be due to the reduced effective mass in $Ca_5Ga_2Sb_6$: when acoustic phonons dominates the charge carrier scattering, the quality factor, which determines the zT of optimally doped materials, is given by $B \propto \frac{N_v}{m_i^* \kappa_L}$[29] ($m_i^*$ is the mass of a single hole pocket along the conduction direction and N_v is the number of bands contributing to transport). Note however that the zT improvement in this study is within the generally accepted uncertainty in zT of about 20%.

Compared with optimally Zn-doped $Ca_5Al_2Sb_6$, the zT in Zn-doped $Ca_5Ga_2Sb_6$ is detrimentally affected by minority carriers at high temperature, leading to a lower peak zT. A maximum zT of about 0.35 is reached at 775 K in the samples with $x = 0.05$ and $x = 0.1$ sample. Beyond $x = 0.1$, the maximum zT decreases, suggesting that the optimal doping level for this compound is surpassed. Using an SPB model at 500 K with $m^* = 1.6m_e$, and an intrinsic mobility of 9 cm^2 V^{-1} s^{-1}, we estimate an optimal carrier concentration of ~10^{20} cm^{-3}. This corresponds to the most lightly doped sample ($x = 0.05$), consistent with the experimental results.

Conclusion

In this study, $Ca_5Ga_2Sb_6$ was successfully p-doped with Zn, leading to metallic behavior and greatly improved

thermoelectric properties. The Ga-based material, when optimally doped, exhibits an increased mobility over the Al analogue, attributed to the reduced effective mass predicted by DFT calculations. The reduction in effective mass was also reflected in the measured Seebeck coefficients at 300 K and 500 K; a single band model yielded $m^* = 1.6m_e$ in Zn-doped $Ca_5Ga_2Sb_6$ in contrast to $m^* = 2.0m_e$ in $Ca_5Al_2Sb_6$. Additionally, detrimental effects from the smaller band gap in $Ca_5Ga_2Sb_6$ were observed: minority carrier activation leads to both compensated Seebeck coefficients and bipolar thermal conductivity at high temperatures. The high cost of Ga must also be considered. Ultimately, the improved electronic mobility of the Ga compound yields an increase in zT between 400 and 800 K relative to the Al analogue. However, due to the reduced band gap, and hence reduced Seebeck coefficient and high bipolar thermal conductivity, of $Ca_5Ga_{1-x}Zn_xSb_6$, the peak zT is lower than the Al analogue.

The authors declare no competing financial interest.

Acknowledgements

We would like to thank the Jet Propulsion Laboratory and the National Science Foundation for their generous support.

References

1 L. E. Bell, *Science*, 2008, **321**, 1457–1461.
2 F. J. DiSalvo, *Science*, 1999, **285**, 703–706.
3 G. J. Snyder and E. S. Toberer, *Nat. Mater.*, 2008, **7**, 105–114.
4 S. M. Kauzlarich, S. R. Brown and G. J. Snyder, *Dalton Trans.*, 2007, 2099–2107.
5 E. S. Toberer, A. F. May and G. J. Snyder, *Chem. Mater.*, 2010, **22**, 624–634.
6 G. A. Slack, *Solid State Physics*, Academic Press, New York, 1979.
7 E. S. Toberer, A. Zevalkink and G. J. Snyder, *J. Mater. Chem.*, 2011, **21**, 15843–15852.
8 S. M. Kauzlarich, *Chemistry, Structure, and Bonding of Zintl Phases and Ions*, Wiley-VCH, 1996.
9 A. M. Mills, R. Lam, M. J. Ferguson, L. Deakin and A. Mar, *Coord. Chem. Rev.*, 2002, **233**, 207–222.
10 G. Cordier, H. Schäfer and M. Stelter, *Z. Naturforsch., B: Anorg. Chem., Org. Chem.*, 1986, **33**, 5–8.
11 T. H. Yi, C. A. Cox, E. S. Toberer, G. J. Snyder and S. M. Kauzlarich, *Chem. Mater.*, 2010, **22**, 935–941.
12 S. R. Brown, S. M. Kauzlarich, F. Gascoin and G. J. Snyder, *Chem. Mater.*, 2006, **18**, 1873–1877.
13 A. F. May, E. S. Toberer, A. Saramat and G. J. Snyder, *Phys. Rev. B: Condens. Matter Mater. Phys.*, 2009, **80**, 125205.
14 B. C. Sales, D. Mandrus and R. K. Williams, *Science*, 1996, **272**, 1325–1328.
15 E. S. Toberer, A. F. May, B. C. Melot, E. Flage-Larsen and G. J. Snyder, *Dalton Trans.*, 2010, **39**, 1046–1054.
16 H. Zhang, J. T. Zhao, Y. Grin, X. J. Wang, M. B. Tang, Z. Y. Man, H. H. Chen and X. X. Yang, *J. Chem. Phys.*, 2008, **129**, 164713.
17 F. Gascoin, S. Ottensmann, D. Stark, S. M. Haile and G. J. Snyder, *Adv. Funct. Mater.*, 2005, **15**, 1860–1864.
18 X.-J. Wang, M.-B. Tang, H.-H. Chen, X.-X. Yang, J.-T. Zhao, U. Burkhardt and Y. Grin, *Appl. Phys. Lett.*, 2009, **94**, 092106.
19 E. S. Toberer, A. Zevalkink, N. Crisosto and G. J. Snyder, *Adv. Funct. Mater.*, 2010, **20**, 4375–4380.
20 A. Zevalkink, E. S. Toberer, W. G. Zeier, E. Flage-Larsen and G. J. Snyder, *Energy Environ. Sci.*, 2011, **4**, 510–518.
21 A. Zevalkink, W. G. Zeier, G. S. Pomrehn, E. Schechtel, W. Tremel and G. J. Snyder, *Energy Environ. Sci.*, 2012, 9121–9128.
22 G. Cordier, E. Czech, M. Jakowski and H. Schäfer, *Rev. Chim. Miner.*, 1981, **18**, 9–18.
23 G. Cordier, H. Schäfer and M. Stelter, *Z. Naturforsch., B: Anorg. Chem., Org. Chem.*, 1986, **33**, 5–8.
24 A. Zevalkink, G. S. Pomrehn, S. Johnson, J. Swallow, Z. M. Gibbs and G. J. Snyder, *Chem. Mater.*, 2012, **24**, 2091–2098.
25 A. Zevalkink, E. S. Toberer, T. Bleith, E. Flage-Larsen and G. J. Snyder, *J. Appl. Phys.*, 2011, **110**, 013721.
26 A. Zevalkink, J. Swallow and G. J. Snyder, *J. Electron. Mater.*, 2012, **41**, 813–818.
27 K. A. Borup, E. S. Toberer, L. D. Zoltan, G. Nakatsukasa, M. Errico, J. P. Fleurial, B. B. Iverson and G. J. Snyder, *Rev. Sci. Instrum.*, 2012, **83**, 123902.
28 S. Iwanaga, E. S. Toberer, A. LaLonde and G. J. Snyder, *Rev. Sci. Instrum.*, 2011, **82**, 063905.
29 Y. Pei, A. D. LaLonde, H. Wang and G. J. Snyder, *Energy Environ. Sci.*, 2012, **5**, 7963–7969.
30 A. Zunger, *Appl. Phys. Lett.*, 2003, **83**, 57–59.
31 Y. I. Ravich, B. A. Efimova and I. A. Smirnov, *Semiconducting Lead Chalcogenides*, Plenum, New York, 1970.
32 H. J. Goldsmid and J. W. Sharp, *J. Electron. Mater.*, 1999, **28**, 869–872.
33 D. G. Cahill and R. O. Pohl, *Annu. Rev. Phys. Chem.*, 1988, **39**, 93–121.
34 D. G. Cahill, S. K. Watson and R. O. Pohl, *Phys. Rev. B: Condens. Matter Mater. Phys.*, 1992, **46**, 6131–6140.